



ELSEVIER

Contents lists available at ScienceDirect

International Journal of Disaster Risk Reduction

journal homepage: www.elsevier.com/locate/ijdr

Using rapid damage observations for Bayesian updating of hurricane vulnerability functions: A case study of Hurricane Dorian using social media

Jens A. de Bruijn^{a,b,*}, James E. Daniell^{a,c}, Antonios Pomonis^a,
Rashmin Gunasekera^a, Joshua Macabuag^a, Marleen C. de Ruiter^b,
Siem Jan Koopman^{d,e,f}, Nadia Bloemendaal^b, Hans de Moel^b, Jeroen C.J.H. Aerts^{b,g}

^a World Bank Group, 1818 H St NW, Washington, DC, 20433, USA

^b Institute for Environmental Studies IVM, VU University, Amsterdam, the Netherlands

^c Geophysical Institute and Center for Disaster Management and Risk Reduction Technology, Karlsruhe Institute of Technology, Karlsruhe, Germany

^d Department of Econometrics and Data Science, School of Business and Economics, Vrije Universiteit Amsterdam, the Netherlands

^e CREATES, Aarhus University, Denmark

^f Tinbergen Institute Amsterdam, the Netherlands

^g Deltares, Delft, the Netherlands

ARTICLE INFO

Keywords:

Vulnerability curves
Social media
Bayesian updating
Rapid damage assessment
Hurricane Dorian
UAVs

ABSTRACT

Rapid impact assessments immediately after disasters are crucial to enable rapid and effective mobilization of resources for response and recovery efforts. These assessments are often performed by analysing the three components of risk: hazard, exposure and vulnerability. Vulnerability curves are often constructed using historic insurance data or expert judgments, reducing their applicability for the characteristics of the specific hazard and building stock. Therefore, this paper outlines an approach to the creation of event-specific vulnerability curves, using Bayesian statistics (i.e., the zero-one inflated beta distribution) to update a pre-existing vulnerability curve (i.e., the prior) with observed impact data derived from social media. The approach is applied in a case study of Hurricane Dorian, which hit the Bahamas in September 2019. We analysed footage shot predominantly from unmanned aerial vehicles (UAVs) and other airborne vehicles posted on YouTube in the first 10 days after the disaster. Due to its Bayesian nature, the approach can be used regardless of the amount of data available as it balances the contribution of the prior and the observations.

1. Introduction

Natural hazards, such as tropical cyclones [1], floods [2] and earthquakes [3], affect millions of people and cost billions of dollars in damages every year. Their impacts are expected to increase further [4] often attributed to factors such as climate change [5] and increasing exposure [6]. Damage assessment immediately after a natural disaster is crucial to enable rescue and relief organizations to mobilize resources for response and recovery processes [7]. However, detailed and accurate assessments often take months to complete

* Corresponding author. IVM, Vrije Universiteit Amsterdam, Faculty of Science, NU building, 8th floor, Wing A, De Boelelaan 1111, 1081 HV, Amsterdam, the Netherlands.

E-mail address: jens.de.bruijn@vu.nl (J.A. de Bruijn).

<https://doi.org/10.1016/j.ijdr.2022.102839>

Received 21 September 2021; Received in revised form 28 January 2022; Accepted 2 February 2022

Available online 5 February 2022

2212-4209/© 2022 The Authors. Published by Elsevier Ltd. This is an open access article under the CC BY license

(<http://creativecommons.org/licenses/by/4.0/>).

[8]. Therefore, the World Bank has recently employed the Global RAPid post-disaster Damage Estimation (GRADE) approach to rapidly estimate damages to physical assets after major disasters [9].

Damage estimations are commonly modelled using the three components of risk: hazard, exposure and vulnerability [10]. Hazard is defined as a potentially damaging event, exposure as the elements subject to damage and losses as a result of a hazard and vulnerability as “the conditions determined by physical, social, economic and environmental factors or processes which increase the susceptibility of an individual, a community, assets or systems to the impacts of hazards” [11]. Vulnerability and fragility functions are commonly used to model damage to buildings due to natural disasters. These functions typically relate a measure of impact, such as wind speed [12], water depth [13] or ground motion [14], to damage. These relations are mostly based on component-based engineering approaches, previous insurance claims, experiments or expert judgment and are often only applicable to particular hazard characteristics and specific built environments [15–18]. For wind damage, these curves often form a shape similar to a cumulative lognormal distribution, where almost no damage occurs at low wind speeds, followed by a rapid increase in potential damage at a specific value for wind speed. This means that small judgement errors in a curve often leads to larger errors in the ultimate damage assessment. In addition, because wind fields are often uncertain, damage estimations based on curves that were not specifically designed for that wind field, are prone to cascading errors in the final damage estimate.

Observations, such as those from surveys [19], can improve the accuracy of damage estimates [17]. However, affected areas are often difficult to access following a disaster [20], and human resources are often limited [21]. Data sources such as social media [7], unmanned aerial vehicles (UAVs) [22] and other remote sensing techniques can provide detailed observations of damage quickly during and after a disaster. However, the amount of data is heavily dependent on the characteristics of the disaster area, such as the number of people that are able to use social media [23,24] and cultural differences [25].

A scientific challenge is to seek methods that use observations from the affected area to improve vulnerability curves. A method that can employ observational data to update prior beliefs (e.g., beliefs based on expert judgment), is Bayesian analysis [26]. The balance between prior information and observational data depends on the number of observations and the level of uncertainty in both the observations and the prior beliefs.

Bayesian updating of fragility functions (i.e., the probability of exceeding a certain damage state) has been employed in numerous studies. For example, Li et al. [14] combined results from numerical simulations and experimental testing of bridge substructures with Bayesian updating to obtain improved earthquake fragility functions. Mishra et al. [27] updated and quantified the uncertainty of analytical hurricane fragility functions for wood-frame buildings with experimental data. In another study, a Bayesian framework was designed to create fragility functions for earthquakes [26]. However, from a risk management perspective, vulnerability functions (where damage is represented as a damage ratio) are more desirable, as they measure the susceptibility to damage of the built environment as a whole [28].

In this paper, we aim to improve existing vulnerability functions employed in GRADE assessments by updating these functions with post-disaster observations using Bayesian zero-one inflated beta regression [29]. The method is applied to a case study of tropical cyclone wind damage in the Bahamas caused by Hurricane Dorian in September 2019. The observations were obtained from online media reports (i.e., YouTube) in the days following the disaster. This data includes some ground observations from driving cars but is mostly composed of observations from UAVs and videos shot from other airborne vehicles. In the remainder of this paper, we describe the general methodology (Sect. 2) and its application to the Bahamas (Sect. 3). We also discuss the applicability of the proposed method to other disaster types and different data sources.

2. Methodology

Bayesian updating or inference refers to the process of updating existing knowledge for a set of n parameters Θ , defined as $\Theta = (\theta_1, \dots, \theta_n)$ and expressed in a prior distribution, defined as $P(\Theta)$, with new information X to find the posterior distribution, defined as $P(\Theta|X)$. Mathematically, we can express Bayesian updating as

$$P(\Theta|X) \propto P(X|\Theta) * P(\Theta). \quad (1)$$

The posterior distribution $P(\Theta|X)$ is obtained by multiplying the prior distribution $P(\Theta)$ by the likelihood distribution $P(X|\Theta)$, which is the probability of observing X given parameter set Θ , and a normalizing constant. The normalizing constant $P(X)$ is omitted here since this is automatically determined during the process of Gibbs sampling (see below; [30,31]).

Following the Bayesian framework, the prior distribution $P(\Theta)$ for vulnerability must be defined. The vulnerability of the building stock can be expressed as a curve that maps wind speed as the explanatory variable (v_1, \dots, v_n) to a damage ratio from 0 to 1 (inclusive) as the response variable (y_1, \dots, y_n). Fragility curves of individual components of buildings (e.g., roof sheathing and nails) are widely regarded as following a cumulative lognormal distribution [32–34]. Assuming identical fragility curves for individual components and independence of failure, a vulnerability curve for a building follows that same cumulative lognormal distribution [35]:

$$y = \Phi\left(\frac{\ln(v/\alpha)}{\beta}\right) \quad (2)$$

where $y \in (0, 1)$ is the damage ratio, α the median capacity (i.e., the wind speed at which buildings are expected to sustain 50% of damage on average) of the building stock, β the logarithmic standard deviation of that capacity, $\Phi(\cdot)$ the cumulative probability density function for the standard normal distribution and v the sustained wind speed. While α and β can be expressed deterministically, we prefer to regard both parameters as uncertain and we express them as the random variables θ_1 and θ_2 , respectively.

In contrast to fragility curves, which model the probability of failure (often through a binary logistic regression), we require a

regression that takes proportional data. For this purpose, the beta distribution is often used as the basis for the likelihood function $P(X|\Theta)$ [36] because it supports a wide range of shapes on the interval (0, 1). Its probability density function, re-parameterized in terms of mean μ and precision φ , is given by Ferrari and Cribari-Neto [37]:

$$f_{\text{beta}}(y; \mu, \varphi) = \frac{\Gamma(\varphi)}{\Gamma(\mu\varphi)\Gamma((1-\mu)\varphi)} y^{\mu\varphi-1} (1-y)^{(1-\mu)\varphi-1}, \quad y \in (0, 1) \tag{3}$$

where $\Gamma(\cdot)$ is the gamma function.

However, observations of the damage ratio can be true values of zero (i.e., no damage) and one (i.e., complete destruction), which are not supported by the beta distribution. In fact, such observations are more frequent because the assumption that the individual building components of buildings fail independently does not always hold. For example, houses are often completely destroyed (i.e., damage ratio of 1) due to the collapse of an important fundament [38] or complete displacement of the entire building [39]. By contrast, houses may be completely undamaged due to their environment or protection measures, such as shielding by other standing buildings [38]. Using the zero-one inflated beta distribution enables us to explicitly model these 0 and 1 observations through probabilities π_0 and π_1 , respectively.

Therefore, for proportional response variables $y_i \in [0, 1]$, Ospina and Ferrari [29] propose a zero-one inflated beta regression. Here, the response variable (y_1, \dots, y_n) is modelled as a mixture probability function of π_0 , the probability that $y = 0$; π_1 , the conditional probability $\Pr(y = 1 | y \neq 0)$; and the beta distribution with expected value μ_y and precision φ for the values between 0 and 1 (0 – 1). Its probability density function is given by:

$$f_{\text{ZOIB}}(y; \pi_0, \pi_1, \mu, \varphi) = \begin{cases} \pi_0 & \text{if } y = 0 \\ (1 - \pi_0)\pi_1 & \text{if } y = 1 \\ (1 - \pi_0)(1 - \pi_1)f_{\text{beta}}(y; \mu_y, \varphi) & \text{if } y \in (0, 1) \end{cases} \tag{4}$$

By employing this distribution with proper parameterization (Sect. 3.3), we can model a process where it is highly probable that the damage ratio is 0 for low wind speed and 1 for high wind speed. For a wind speed in between, it is likely that y is modelled on the continuous scale (0–1) through the beta distribution. We base the equation for μ_y on Eq. (2) presented above:

$$\mu_y = \Phi\left(\frac{\ln(v/\theta_1)}{\theta_2}\right) \tag{5}$$

For probabilities π_0 and π_1 we specify a linear relationship with v on the logit scale as follows:

$$\pi_0 = \text{logit}^{-1}(\theta_3 + \theta_4 v) \tag{6}$$

$$\pi_1 = \text{logit}^{-1}(\theta_5 + \theta_6 v) \tag{7}$$

In Eqs. (5)–(7), the parameters $\theta_1, \dots, \theta_6$ are assumed to come from normal distributions with some mean and standard deviation.

Finally, the prior distribution (Eqs. (4)–(7)) and parameters $(\theta_1, \dots, \theta_6)$ can be updated with some observations with the wind speed as the explanatory variable (v_1, \dots, v_n) and the corresponding response variables (y_1, \dots, y_n) using Gibbs sampling, which is a Markov chain Monte Carlo (MCMC) algorithm, see Gilks et al., [30]; for a general treatment. For the purpose of Gibbs sampling, the predictor variable v is normalized such that $\tilde{v} \in (0, 1]$ by dividing v by the maximum observed wind speed (i.e., $\max(v)$). All other input variables are scaled accordingly. Then, samples of the posterior distribution are generated using the Just Another Gibbs Sampler program (JAGS; [40]). We first use 1000 iterations to tune the samplers (i.e., adaptation), 1000 iterations as a burn-in to find the place where the Markov chain is most representative of the sampled distribution, followed by 100,000 iterations in three chains with a thinning of 100.

To verify the convergence of the Markov chains, we can present different diagnostics which are reviewed in, amongst others, Cowles and Carlin [41] and Brooks and Roberts [42]. In particular, we concentrate on diagnostics based on distributional and autocorrelation statistics.

3. Case study of Hurricane Dorian

In this section, the methodology for updating vulnerability curves described above is applied to a rapid damage estimation of Hurricane Dorian in Grand Bahama and the Abaco Islands, the northernmost main islands of the Bahamas. First, the hazard (Sect. 3.1) and exposure components (Sect. 3.2) are briefly described. Then, we discuss the collection of observations for the vulnerability component and the Bayesian updating process (Sect. 3.3). Finally, these three components of risk are combined to obtain a final damage estimate (Sect. 3.4). It should be noted that all data sources had to have been collectible in the first 10 days following the first landfall of the Hurricane in the Bahamas to be eligible for the rapid damage estimate.

3.1. Hazard

On August 24, 2019, Tropical Storm Dorian formed over the Atlantic Ocean and began tracking through the Windward Islands and the U.S. Virgin Islands towards the Bahamas [43]. On 1 September, Dorian reached Category-5 strength with maximum sustained wind speeds exceeding 300 km/h. At 16:40 UTC that day, Dorian made landfall at Elbow Cay, Great Abaco, in the Bahamas. During its passage over the Great Abaco and Grand Bahama islands, the weakening of the nearby high-pressure area caused the hurricane to lose

its steering currents and therefore significantly slowing its forward speed to 2 km/h, at times even coming to a standstill. Dorian remained near-stationary for 36 h, until the hurricane started moving north-northwestwards towards North Carolina (USA). Dorian dissipated on 8 September near Canada.

In this study, meteorological conditions during Hurricane Dorian's passage over the Bahamas is taken from the International Best Track Archive for Climate Stewardship (IBTrACS; [44]). Using the position of the eye, the minimum pressure, maximum wind speed, and size of the eye (i.e., radius to maximum winds) the 2D wind field is constructed by applying the parametric approach of Holland [45]; which was further refined in by Lin and Chavas [46]. To obtain the wind field at 10 m above surface level (Fig. 1) a reduction factor of 0.85 is applied [47].

3.2. Exposure

To determine the exposure of the residential buildings on the Abaco and Grand Bahama Islands, we consulted the 2000 and 2010 Population and Housing Census of the Bahamas [48,49]. The census contains information about the housing stock. Specifically, it contains data on residential buildings and occupied and vacant dwelling units for each settlement and enumeration district in the Abaco Islands and each supervisory district in Grand Bahama, as well as the number of bedrooms and the total annual household income for each household size. In the Abaco Islands (and to a lesser extent in Grand Bahama), the proportion of vacant housing stock is relatively high as the islands are a tourist destination, and many homes are owned or rented by vacationers. The Abaco Islands also has many migrant communities (mainly working in the service sectors for the tourism industry), who reside in low-quality housing in several informal settlements, such as the Mudd and the Pigeon Peas settlements. Other settlements are occupied by the local Bahamian population, while tourists and foreign citizens, often reside in high-value homes and resorts.

To account for this heterogeneity 11 settlements (for Grand Bahamas) and 31 enumeration districts (for Abaco), based on available census data, were mapped individually and the value of residential buildings within three building classes (low-, medium- and high-quality) was estimated for each region. We first estimated the number and area of buildings per building type in each region. To do so, we consulted building footprints from OpenStreetMap (and found 16,100 and 12,500 building footprints in Grand Bahama and the Abaco Islands respectively). We estimated the housing stock in 2019 by projecting data from the 2000 and 2010 census onto 2019, taking official population projections into account [50] and estimated the floor area of the dwellings using data on the number of bedrooms per dwelling. We also consulted the Bahamas 2013 Household Expenditure Survey [51], which provided information about household consumption quintiles and housing conditions, such as type of dwelling, number of rooms, bedrooms, period of construction of the dwelling, type of tenure, type of construction material used for the outer walls, the roof cover and the floors.

Next, we estimated the unit cost of construction of the building classes based on housing prices provided by real estate agents, building contractors and a census of informal settlements in the Abaco Islands [52]. Finally, we consulted the Annual Building Construction Statistics Reports (e.g. Ref. [53]), which contain data on the investment values of newly constructed buildings. Fig. 2 shows the reported monetary value of low-quality residential buildings per region (Fig. A1 and A2 for values of medium- and

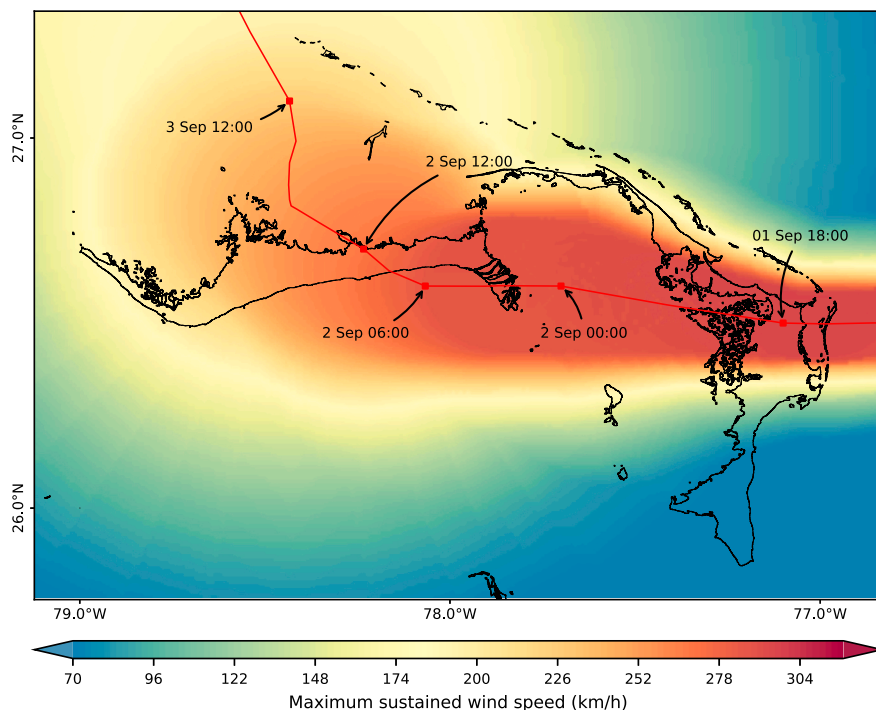


Fig. 1. Maximum 1-min average sustained wind speeds at 10 m above surface level at 0.01° resolution for Hurricane Dorian during its passage over the Bahamas in September 2019. Time stamps are given in UTC.

high-quality buildings; note the adjusted scales). Note that these estimations do not include building content. Since no official maps of the regions were available, we determined the coordinates of the population centres for each region. All maps are presented as Voronoi diagrams (i.e., partitioned into regions closest to each centre point) based on these centroids.

3.3. Vulnerability

To estimate event-specific vulnerability curves, we aimed to update vulnerability curves derived from previous hurricane observations in similar built environments using damage observations for individual buildings in the affected area. Therefore, we analysed all 498 YouTube videos that were listed when we searched for “Bahamas Dorian” and that were posted in the 10 days after the first landfall of Hurricane Dorian in the Bahamas (September 1st–9th). We then analysed all videos that 1) showed an overview of an area or a row of buildings to ensure the sample was as representative as possible (Appendix B), 2) that we were able to geotag (i.e., locate) and 3) that showed buildings that did not appear to have undergone extensive flood damage. This resulted in a set of 15 videos (Appendix C), from which we extracted 732 buildings. Fig. 3 depicts two examples of buildings extracted from the videos. By comparing the footage with satellite imagery of the area before the hurricane, we ensured that all buildings in an observed area or row of buildings were analysed, including those that completely disappeared in the storm.

Then, the damage ratio [0–1] and building class (i.e., low-, medium-, and high-quality) was estimated for each building. The assessment was performed by three independent experts, because the assessment of building classes and damages from images can be up for interpretation, leading to a measurement error. While several scales for building damages were previously developed (e.g. Refs. [54,55], these do not directly translate into a damage ratio. Therefore, the damage was estimated based on the damage seen in the value of subcomponents of the structure and their relative values and interactions as a whole, see Massarra et al. [56]. In some areas, especially those with low-quality houses, it was difficult to extract an image of each individual building due to the large amount of destruction and displacement, and/or difficulty in extracting a picture of each individual house. In such cases, we estimated the number of buildings by comparison to pre-event satellite imagery. Then, the individual judges assigned fractions of damage levels and building classes. Subsequently, the fractions were ranked according to their damage levels and translated to individual scores according to the number of buildings. To assess the reliability of the damage assessment, we report the intraclass correlation for the reliability of the average rating of the damage ratios for a random sample of k raters [57] and the Fleiss kappa score [58] for the building classes.

The median damage ratio and building class were then used in further analysis. Buildings were discarded when either 1) one of the experts deemed the picture or scene too unclear to make a proper assessment or 2) in the rare case when all experts assigned a different building class. This resulted in 727 damages for individual buildings of which 241, 387 and 99 buildings are in the low-, medium- and high-quality building classes, respectively. The intraclass correlation is 0.931 for de building damages and the Fleiss kappa score for building class is 0.47.

Next, we derived a prior (i.e., a vulnerability curve based on pre-existing knowledge; Sect. 2) for each building class by estimating the parameters based on expert judgment of the strength of the buildings in similar built environments. Such curves have fitted the results of previous Post-Disaster Needs Assessments (PDNAs) within the Caribbean for stronger wind events for economic damage, and provide similar smoothed curves to existing models in the region such as those presented in the UNDRR’s Global Assessment Report on Disaster Risk Reduction [59] for developed locations. Fig. 4 (left) shows the parameters α and β of these curves for the three housing qualities and Fig. 4 (right) shows the associated damage ratio for low-quality buildings in the affected region.

We then set the priors (Fig. 5) for μ_{θ_1} and μ_{θ_2} (Eq. (5)) using the specified values of α and β for each building class; σ_{θ_1} was set to 15 using the uncertainty range expressed in the fragility curves for a specific damage state (i.e., the range of wind gust speed that causes a specific damage state) in HAZUS (a tool for analysing natural hazards in the United States) for a similar built environment [60] and σ_{θ_2} was set to 0.03 to allow for uncertainty of the building typology. The values of the means and standard deviations of $\theta_3, \dots, \theta_6$ (Eq. (6))

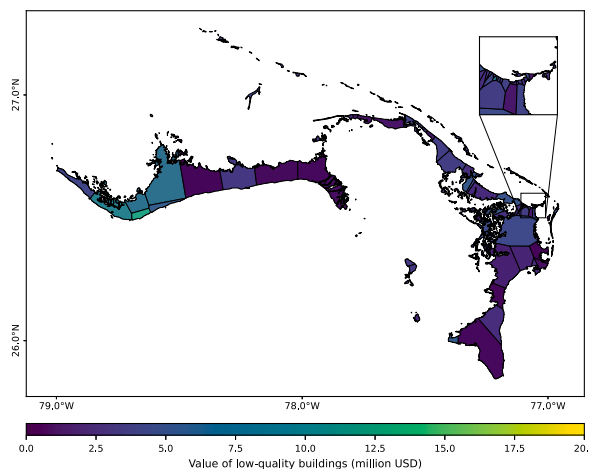


Fig. 2. Value of low-quality buildings per region.



Fig. 3. Footage from “Dorian’s Destruction of Treasure Cay, Abaco Bahamas” (<https://www.youtube.com/watch?v=hvCQdLWW-y4>) containing (left) a medium quality building with structural detailing with roof damage and water intrusion to part of the building’s structure, non-structural damage (ca. 25% damage) and (right) a low quality building (with minor structural detailing), missing its front wall, roof damage, and significant debris (ca. 50% damage).

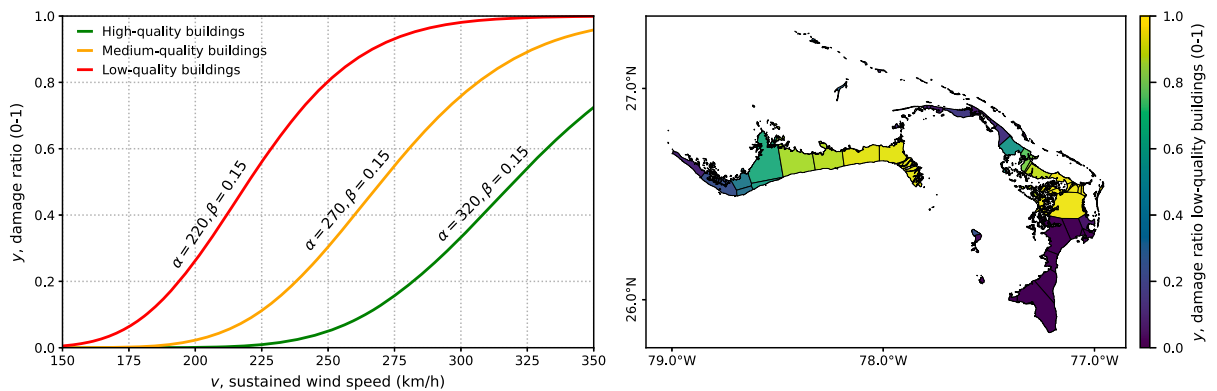


Fig. 4. Vulnerability functions for low-, medium- and high-quality buildings (left) and damage ratios for low-quality buildings in Grand Bahama and the Abaco Islands (right).

and (7)) were set such that the probability π_0 is near one when μ_y is near zero and π_0 near zero when μ_y is near one. Conversely, π_1 is set such that its value is near one when μ_y is near one and π_1 near zero when μ_y is near zero. This is explained in full in Appendix D. For precision parameter φ , we use an uninformed uniform prior.

For each building’s observed damage ratio ($y_1, \dots, y_n \in [0, 1]$), the maximum sustained wind speed (v_1, \dots, v_n) was obtained using the location of the building (Sect. 3.1). Finally, using these observations we performed Gibbs sampling to obtain the posterior distribution (Fig. 5; Sect. 2). In Fig. 5, the upper row (a-c) shows the prior vulnerability curves, whereas the lower row (d-f) shows the posterior curves. From left to right the columns represent the vulnerability curves for low- (a,d), medium- (b,e) and high-quality (c,f) buildings. The red, green and blue colours denote respectively π_0 , π_1 and μ_y . The solid line represents the median (P_{50}), the dashed lines (P_{25-75}) represent the 25th and 75th percentile and the shaded area represents the 10th-90th percentile range.

Comparing the top and the bottom row, the curves for all building types have shifted substantially showing the result of the Bayesian updating. Note that for the posterior vulnerability curves for low-quality buildings (bottom left; d) it might appear that there is a significant probability that the building is entirely destroyed (green curve). However, this is not the case since π_1 is the conditional probability that the damage ratio is one given that the damage ratio is not zero ($Pr(y = 1 | y \neq 0)$; Eq. (4)), and hence the probability that the damage is 0, is much higher. Fig. 6 shows the resulting posterior damage ratio per district for low-, medium- and high-quality buildings. As expected, damage ratios are higher for lower-quality buildings and in districts along the hurricane track.

Finally, figures E1, E2 and E3 display the values per iteration, density plot and autocorrelation for $\theta_1, \dots, \theta_6$ for each building quality class. While most sequences of generated parameters in the MCMC have low autocorrelations, some parameters do show high autocorrelations (i.e., θ_3 and θ_4 for low- and medium-quality buildings and θ_1 and θ_2). This is likely caused by the absence of data information for these parameters, together with a possibly large disagreement between the prior and observed data.

3.4. Damage estimation

Finally, the three components of risk were combined (i.e., hazard \times exposure \times vulnerability) to obtain a damage estimation for residential buildings (Table 1; Fig. 7) of 1056 million USD using the prior vulnerability curves versus an estimate of 912 million USD using posterior curves (i.e., $\sim 14\%$ lower). It should be noted that we used the coordinates of the population centre determined for each

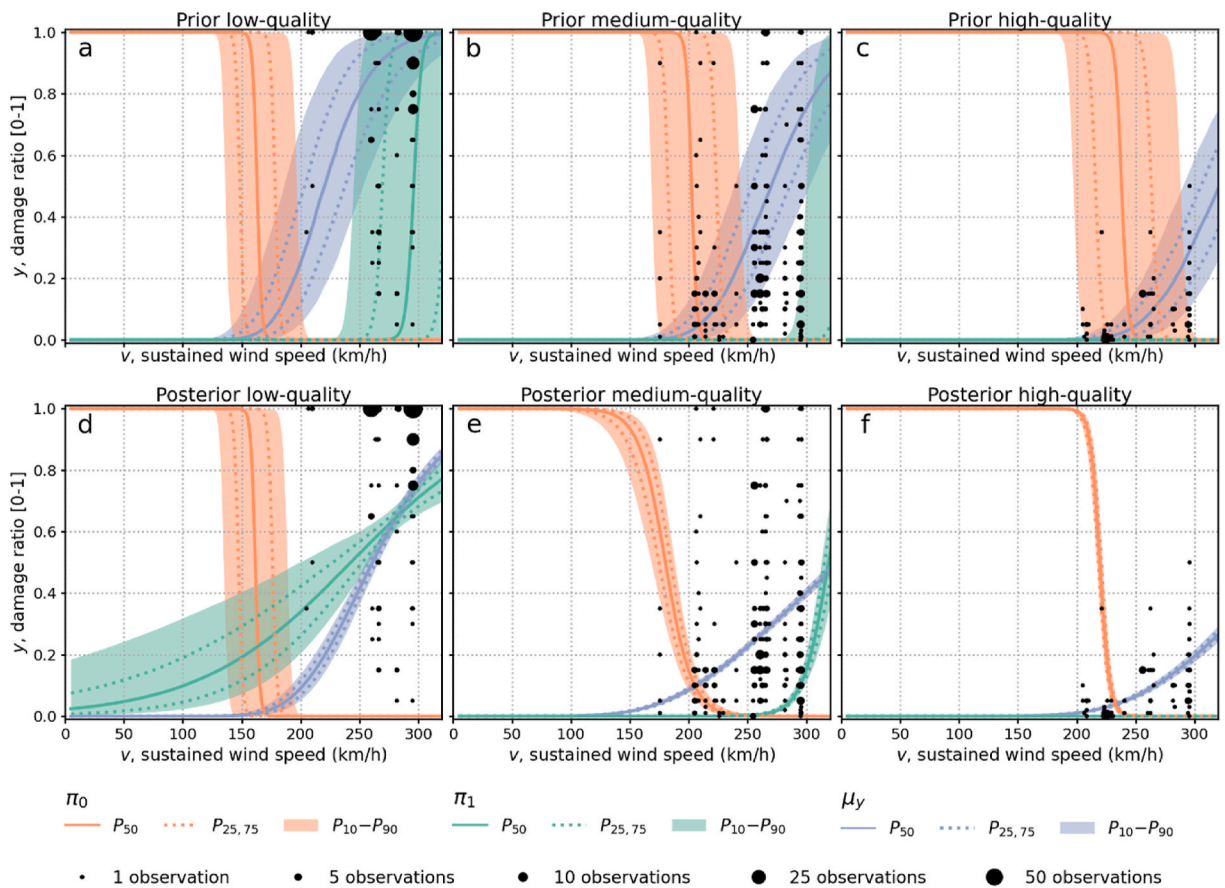


Fig. 5. Visualization of observations, priors and posteriors 25th, 50th (median), 75th percentile and the 10th–90th percentile range for low-, medium- and high-quality buildings.

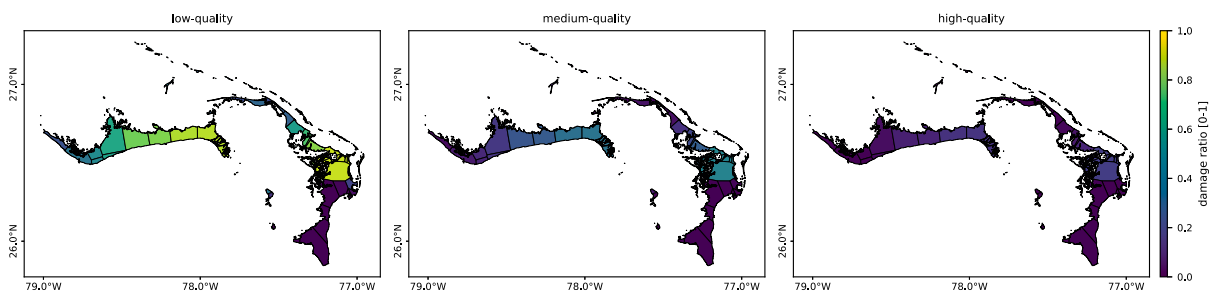


Fig. 6. Posterior damage ratio per district for low-, medium- and high-quality buildings.

region (Sect. 3.2) to extract the wind speed data (Sect. 3.1). In addition, appendix F shows posterior damages where the minimum, median (default) and maximum building quality is taken for each observation, as well as for the minimum, median (default) and maximum damage ratio. A short discussion of the uncertainty is also included.

Table 1
Damage for residential buildings per building class derived from prior and posterior distributions.

	Prior (million USD)	Posterior (million USD)	Percentage change
Low-quality	155	156	+1%
Medium-quality	543	516	−5%
High-quality	359	240	−33%
Total	1056	912	−14%

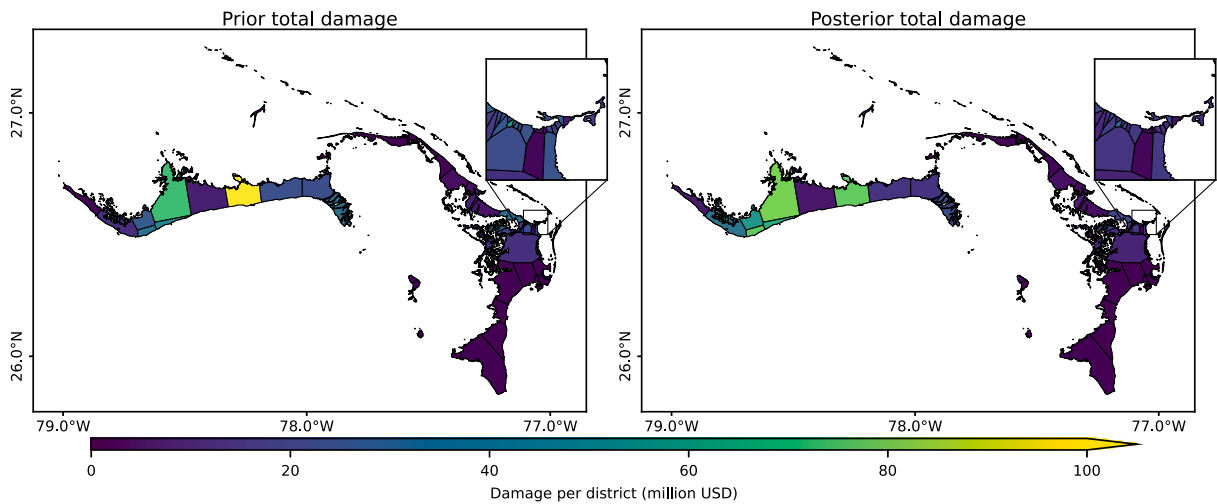


Fig. 7. Damage to low-, medium- and high-quality housing combined derived from prior and posterior vulnerability curves.

4. Discussion and conclusions

In this paper, we present a framework that uses Bayesian updating with social media data (YouTube videos) to create event-specific vulnerability curves. This framework uses the zero-one inflated beta distribution, which allows us to use post-disaster observations to create vulnerability curves that have been adjusted for local hazard and building characteristics. We demonstrate their application in a rapid damage assessment of structural damage to buildings caused by Hurricane Dorian in the Bahamas. In our estimation, wind damage to residential buildings is $\sim 14\%$ lower compared to that calculated using pre-existing vulnerability curves (i.e., the priors). The largest relative difference was found for high-quality buildings.

Unfortunately, validation of the estimated posterior vulnerability curve with a “gold standard” vulnerability curve was not possible. While damage assessments of hurricane Dorian are available [61], no independent wind vulnerability curves are available for hurricane Dorian in the Bahamas to the best of our knowledge. Because 1) the assessed damage is only provided as an overall estimate, 2) that detailed wind and exposure components were not provided, and 3) the fact that this study only considered wind damage, we could not derive a wind vulnerability curve from the damage assessment. Moreover, even if vulnerability curves were available, these also include the uncertainties of the hazard component used in the respective study. This means that vulnerability functions are often characterized as semi-empirical [12,70–72] and direct comparison would be unproductive.

The use of social media data to assess building damages has several limitations. Observations from online media are biased, and some demographic groups have easier access to internet resources than other groups [62]. In addition, observations tend to focus on the most impacted areas, as these are more newsworthy [63]. While we have aimed to reduce this bias by only including footage that showed relatively large areas, we found very little footage of the less severely impacted parts of the islands, such as the northern and southern tips of the Abaco Islands. Moreover, manual analysis of social media data is laborious. In the future, improvements could be made here using automated geolocalization of imagery [64], and damage detection from that imagery [65].

Moreover, the large spread in the observations (Fig. 5) shows that vulnerability is a complex concept. The vulnerability of a single building or part of building to a specific hazard is determined by many factors. In this paper, we only considered sustained wind speed. However, rainfall patterns and other environmental factors could also be important [44,66]. In addition, while we used three different building classes, the real variation in the strength of these buildings cannot be captured by three relatively simple curves.

The variation in building classes was also difficult to capture. While the agreement between judges for the damage ratio is considered excellent [67,68], the agreement for building classes is considered moderate [69]. For our case study, we based our classification of damaged buildings for the most part on post-disaster imagery. While we aimed to deduce the building quality class from the building structure rather than from the damage to the building, it is likely that bias was introduced in the classification. A better approach would be to use pre-disaster imagery (e.g., Google Street View or Mapillary) or, even better, detailed construction data per building. Unfortunately, these were unavailable for the Grand Bahamas and the Abaco Islands.

This was further complicated by the limited availability of vulnerability curves for the specific built environment. The estimated priors are based on a combination of data sources and expert judgement. This likely caused a relatively large disagreement between priors and observations for some parameters, resulting in a high autocorrelation (Fig. E1, E2 and E3). This calls for the establishment of a database of vulnerability curves for hurricane winds that considers a wide range of building typologies and strengths across a wide spectrum of wind intensities.

We applied the method using observations from online media. However, point observations from other sources could also be used. For example, survey data collected by experts or insurance claims would likely be more reliable. However, the availability of such observations from such sources during the first days following a disaster is generally limited, which reduces their applicability for rapid post-disaster damage assessments. Our method could be applied to other hazard types, such as floods and earthquakes. However,

building damage caused by standing water may be more difficult to observe from pictures than structural damage caused by earthquakes. Therefore, for floods additional data, such as data from surveys or insurance reports, may be required.

Code availability

Python and R code is available on GitHub (<https://github.com/jensdebruijn/Bayesian-updating-of-hurricane-vulnerability-functions>).

Data availability

The damage observations and wind field are available on GitHub (<https://github.com/jensdebruijn/Bayesian-updating-of-hurricane-vulnerability-functions>).

Author contribution

JB developed the methodology and took lead in writing the manuscript. JD took part in the creative process and assessed the damage ratios. AP, RG and JM collected and analysed the exposure data. MR assisted in writing the manuscript. SK and HM assisted in development of the methodology. NB created the wind field. JA assisted in writing and oversaw the creative process.

Disclaimer

The findings, interpretations, and conclusions expressed in this paper are entirely those of the authors. They do not necessarily represent the views of the International Bank for Reconstruction and Development/World Bank and its affiliated organizations, or those of its Executive Directors or the governments they represent.

Declaration of competing interest

The authors declare that they have no known competing financial interests or personal relationships that could have appeared to influence the work reported in this paper.

Acknowledgements

Our research was funded by an NWO-Vici grant from the Netherlands Organisation for Scientific Research (NWO; grant number 453-14-006) and an EU-ENHANCE grant from the European Community's Seventh Framework Programme (FP7; grant number 308438). This work was conducted by the World Bank's Disaster Resilience Analytics and Solutions (D-RAS) Knowledge Silo Breaker (KSB), under the Global Practice for Urban, Disaster Risk Management, Resilience and Land (GPURL). This research has been funded by the World Bank and the Global Facility for Disaster Reduction and Recovery (GFDRR) grant (TF0B1140).

Appendices

Appendix A

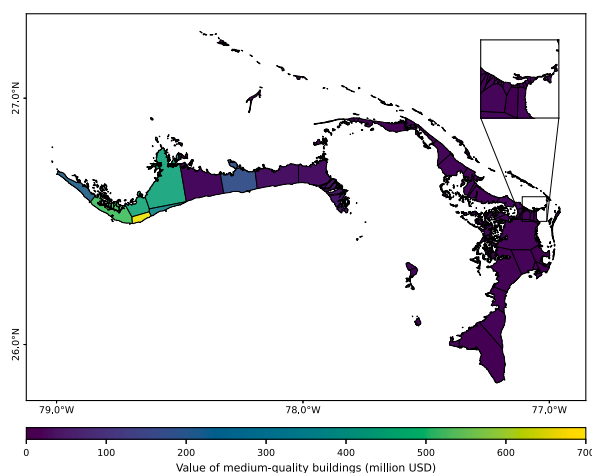


Fig. A1. Value of medium-quality buildings per region. .

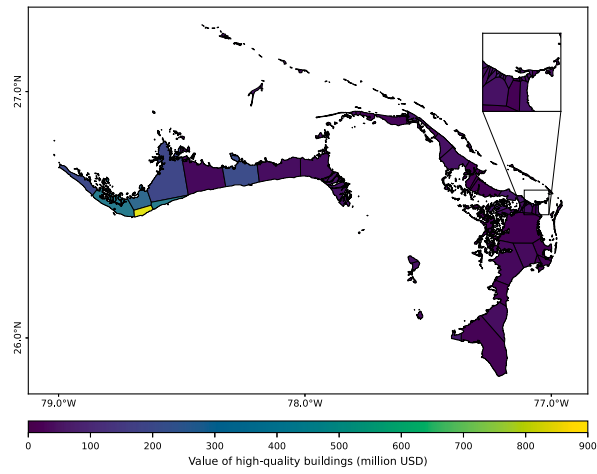


Fig. A2. Value of high-quality buildings per region.

Appendix B

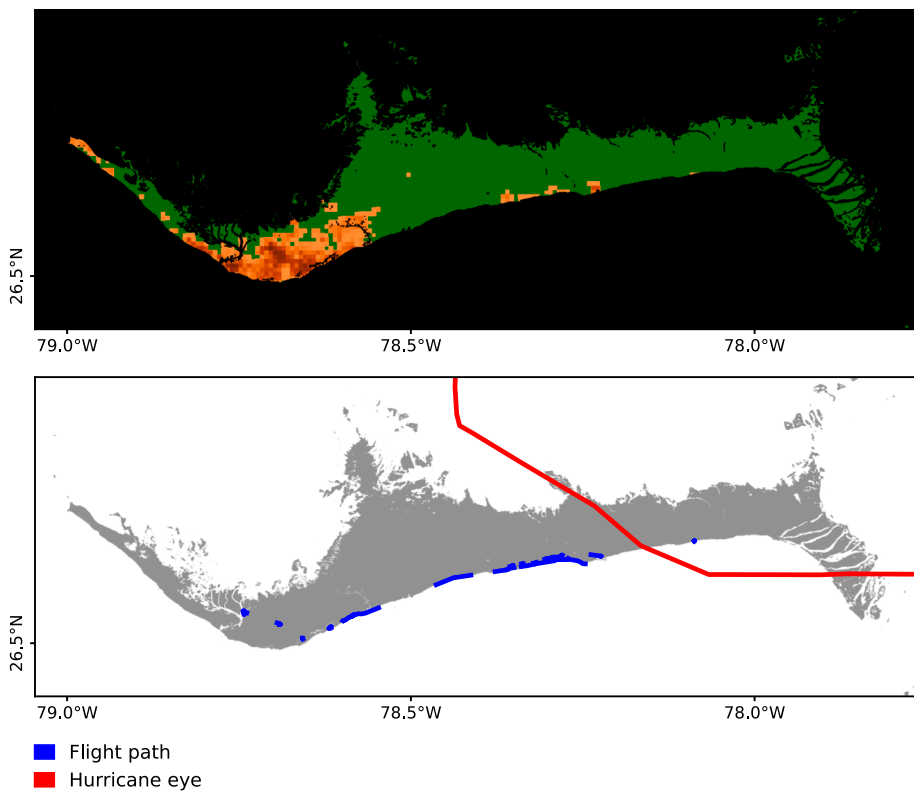


Fig. B1. Flight paths, and heatmap of buildup area from the Global Humans Settlement Layer for Grand Bahama.

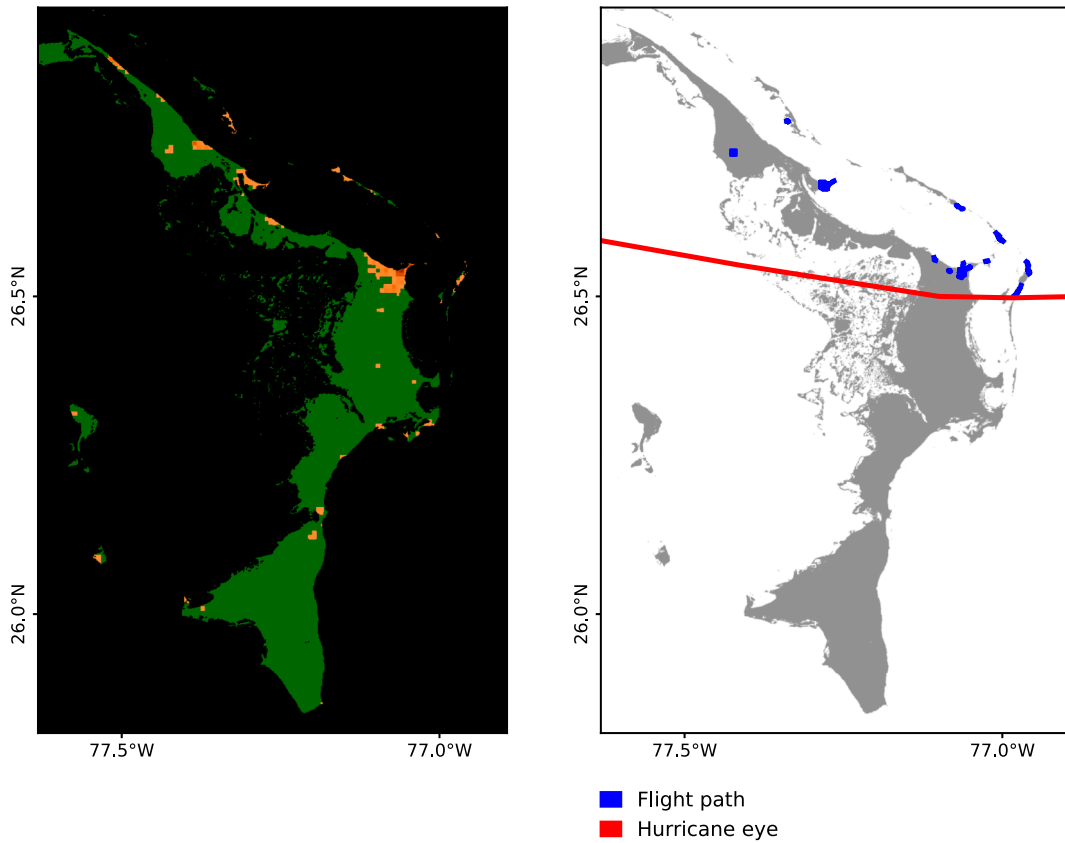


Fig. B2. Flight paths, and heatmap of buildup area from the Global Humans Settlement Layer for Abaco Islands.

Appendix C

- <https://www.youtube.com/watch?v=rq95eJWxpd8>
- <https://www.youtube.com/watch?v=beXg9egFcAs>
- https://www.youtube.com/watch?v=U0omTvsIr_U
- <https://www.youtube.com/watch?v=SuzXtfdZqvg>
- <https://www.youtube.com/watch?v=8QoqtB6HPMY>
- <https://www.youtube.com/watch?v=SN4jgJX0OP8>
- <https://www.youtube.com/watch?v=hvCQTLWW-y4>
- <https://www.youtube.com/watch?v=11lZzCpeIIs>
- <https://www.youtube.com/watch?v=SrUfwnX-UjI>
- <https://www.youtube.com/watch?v=Ar2BdIEI59w>
- <https://www.youtube.com/watch?v=9PypGi8M29Q>
- <https://www.youtube.com/watch?v=mpgGw3iyBPU>
- <https://www.youtube.com/watch?v=AdHombKmG78>
- https://www.youtube.com/watch?v=_tFfnIGq2qE
- <https://www.youtube.com/watch?v=E-zdt-fYlIlg>

Appendix D

μ_{θ_3} and μ_{θ_4} are chosen such that π_0 (i.e., the probability that the damage ratio is zero) is 0.99 where μ_y is 0.01 and π_0 is 0.01 where μ_y is 0.05. In simpler terms this means that the probability that the response variable y_i is a true zero, is near-one when μ_y is also near-zero, and near-zero otherwise (P_{50} or median in Fig. 5). The standard deviation (σ_{θ_3} and σ_{θ_4}) is set at 10% of the mean. Likewise, μ_{θ_5} and μ_{θ_6} are chosen such that π_1 (i.e., the probability that the damage ratio is one) is 0.01 where μ_y is 0.95 and π_1 is 0.99 where μ_y is 0.99. Likewise, the standard deviation (σ_{θ_5} and σ_{θ_6}) is set at 10% of the mean.

Appendix E

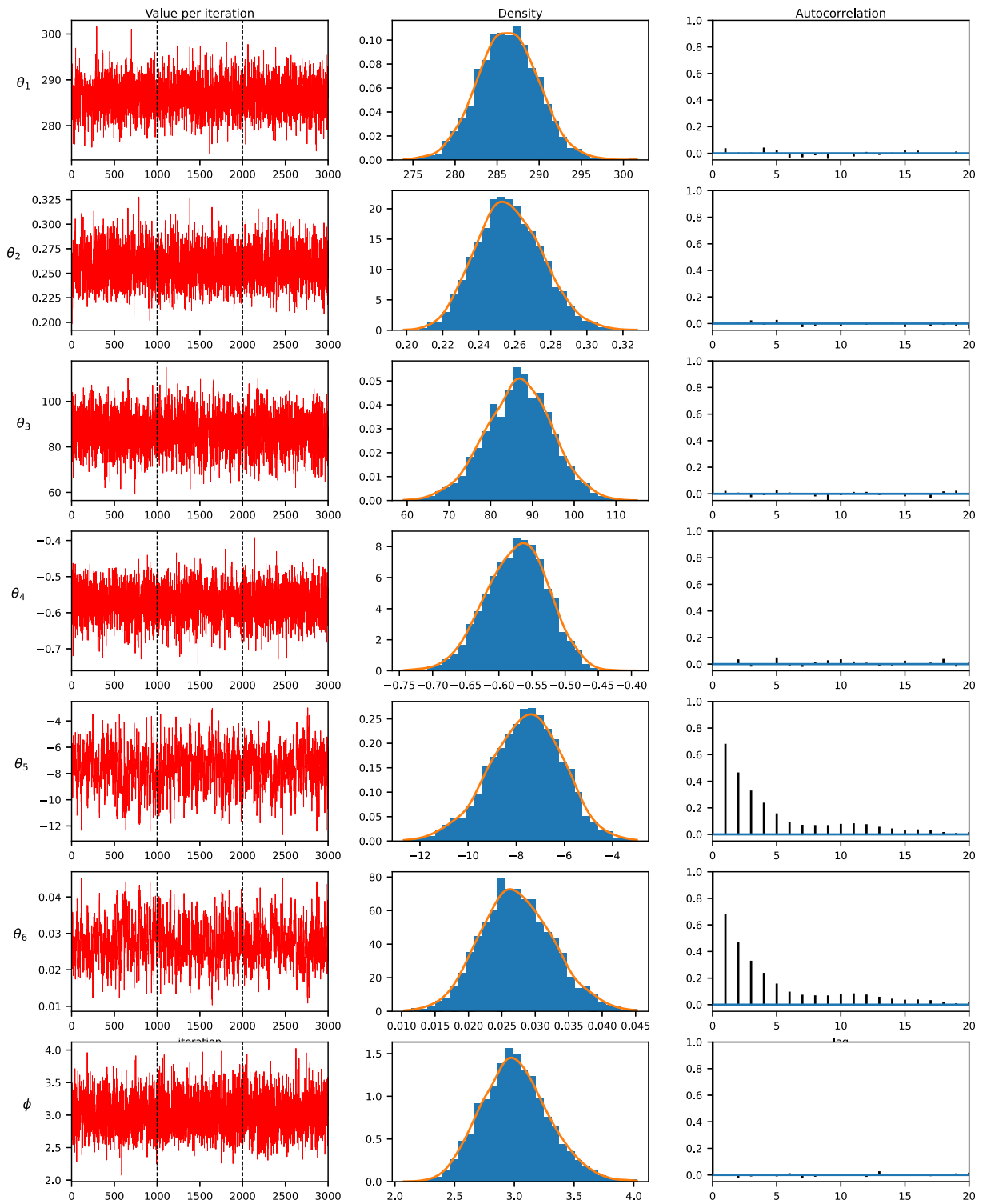


Fig. E1. Values per iteration, density plot and autocorrelation of $\theta_1, \dots, \theta_6$ for low-quality buildings. All values were denormalized after Gibbs sampling. The dashed lines in the top row represent the cut-offs between the 3 chains used in Gibbs sampling.

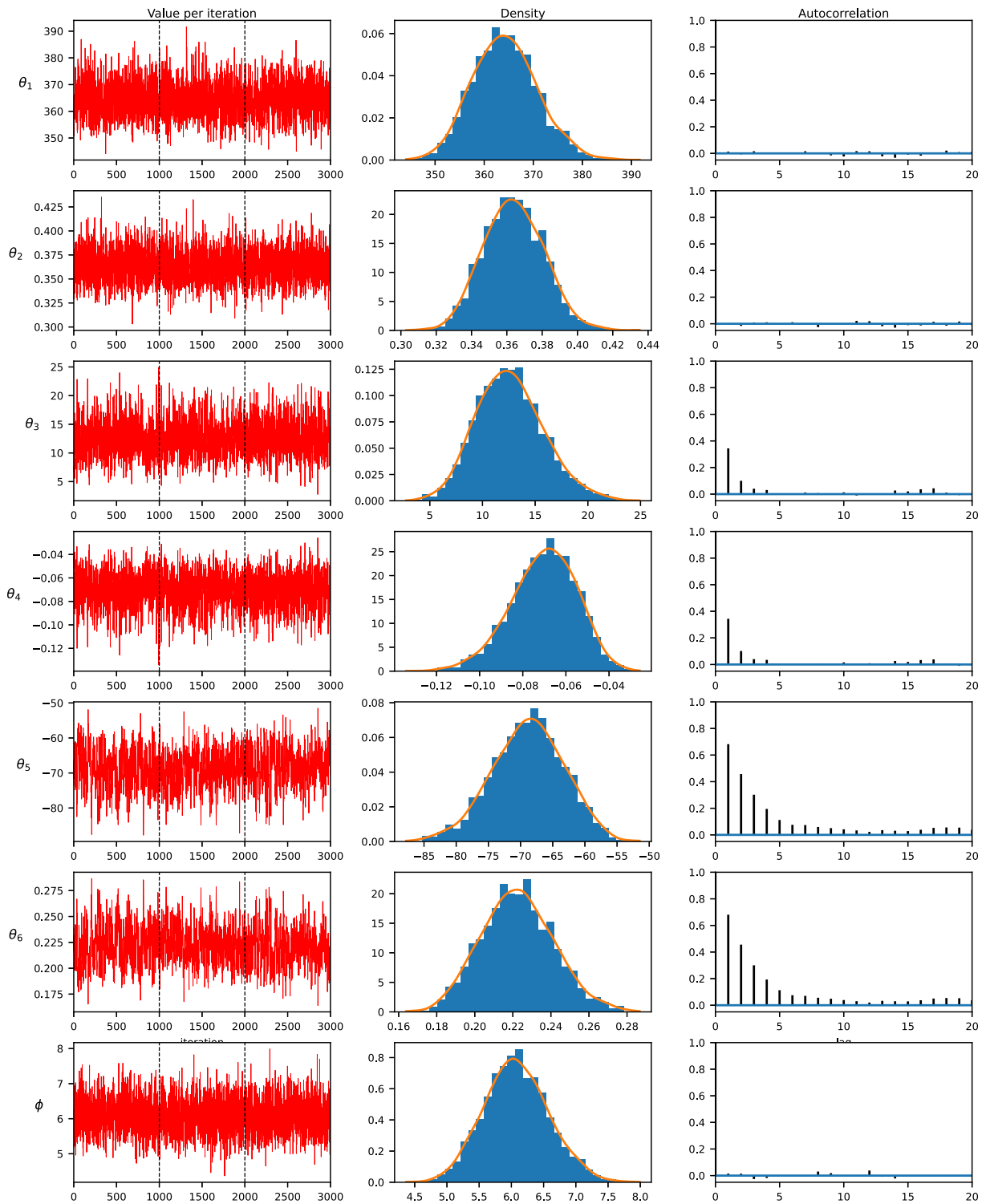


Fig. E2. Values per iteration, density plot and autocorrelation of $\theta_1, \dots, \theta_6$ for medium-quality buildings. All values were denormalized after Gibbs sampling. The dashed lines in the top row represent the cut-offs between the 3 chains used in Gibbs sampling.

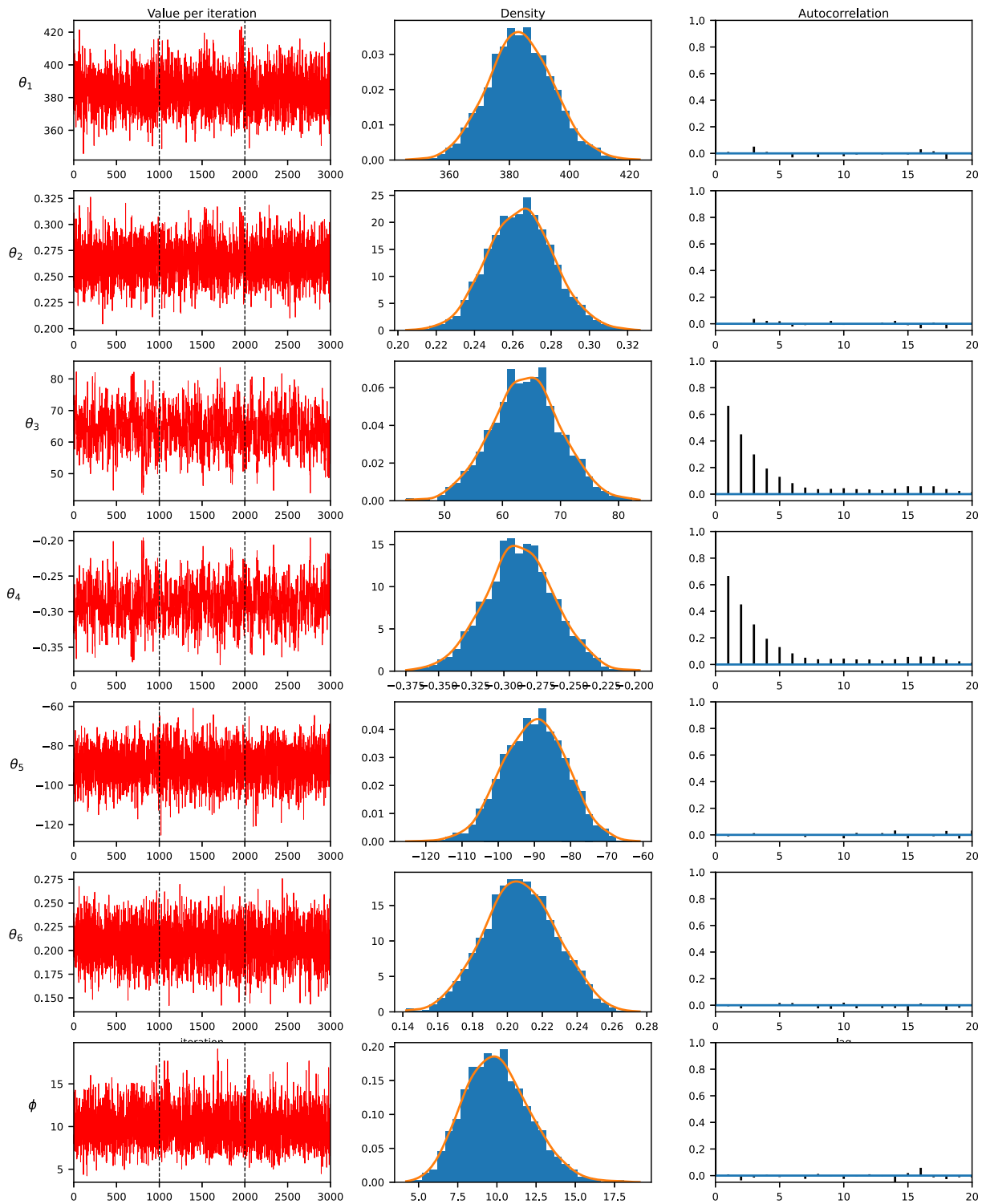


Fig. E3. Values per iteration, density plot and autocorrelation of $\theta_1, \dots, \theta_6$ for high-quality buildings. All values were denormalized after Gibbs sampling. The dashed lines in the top row represent the cut-offs between the 3 chains used in Gibbs sampling.

Appendix F

Building quality stat	Damage ratio stat	Posterior damage (million USD)
minimum	median	1291
maximum	median	705
median	minimum	603
median	maximum	1573

We put this uncertainty into perspective by looking at the uncertainty of the prior vulnerability curve and the wind field. Using our prior the estimated damage is 1056 million USD. When reducing the α -value (equation (2) in the manuscript) by just 10%, the estimated prior damage is 1954 million USD, and when increasing α by 10% estimated prior damage is 541 million USD. This uncertainty is further compounded when considering errors in the wind field. For example, when considering just a 5% error in the wind field in addition to the adjustment of α , the estimated damage ranges from 343 million USD to 2395 million USD. Such an uncertainty of about a factor 7 (in this conservative example) is of similar magnitude as uncertainty in flood damage estimates (see recent overview by Hinkel et al. (2021)).

References

- [1] R. Mendelsohn, K. Emanuel, S. Chonabayashi, L. Bakkensen, The impact of climate change on global tropical cyclone damage, *Nat. Clim. Change* 2 (3) (2012) 205–209, <https://doi.org/10.1038/nclimate1357>.
- [2] H.C. Winsemius, J.C.J.H. Aerts, L.P.H. Van Beek, M.F.P. Bierkens, A. Bouwman, B. Jongman, J.C.J. Kwadijk, W. Ligtoet, P.L. Lucas, D.P. Van Vuuren, P. J. Ward, Global drivers of future river flood risk, *Nat. Clim. Change* 6 (4) (2016) 381–385, <https://doi.org/10.1038/nclimate2893>.
- [3] R. Bilham, The seismic future of cities, *Bull. Earthq. Eng.* 7 (4) (2009) 839–887, <https://doi.org/10.1007/s10518-009-9147-0>.
- [4] S.L. Cutter, A. Ismail-Zadeh, I. Alcántara-Ayala, O. Altan, D.N. Baker, S. Briceño, H. Gupta, A. Holloway, D. Johnston, G.A. McBean, Y. Ogawa, D. Paton, E. Porio, R.K. Silbereisen, K. Takeuchi, G.B. Valsecchi, C. Vogel, G. Wu, Global risks: pool knowledge to stem losses from disasters, *Nature* 522 (7556) (2015) 277–279, <https://doi.org/10.1038/522277a>.
- [5] C. Mora, D. Spirandelli, E.C. Franklin, J. Lynham, M.B. Kantar, W. Miles, C.Z. Smith, K. Freel, J. Moy, L.V. Louis, E.W. Barba, K. Bettinger, A.G. Frazier, Ix Colburn, J.F. N. Hanasaki, E. Hawkins, Y. Hirabayashi, W. Knorr, C.M. Little, K. Emanuel, J. Sheffield, J.A. Patz, C.L. Hunter, Broad threat to humanity from cumulative climate hazards intensified by greenhouse gas emissions, *Nat. Clim. Change* 8 (12) (2018) 1062, <https://doi.org/10.1038/s41558-018-0315-6>.
- [6] L.M. Bouwer, Have disaster losses increased due to anthropogenic climate change? *Bull. Am. Meteorol. Soc.* 92 (1) (2011) 39–46, <https://doi.org/10.1175/2010BAMS3092.1>.
- [7] Y. Kryvasheyev, H. Chen, N. Obradovich, E. Moro, P. Van Hentenryck, J. Fowler, M. Cebrian, Rapid assessment of disaster damage using social media activity, *Sci. Adv.* 2 (3) (2016), e1500779, <https://doi.org/10.1126/sciadv.1500779>.
- [8] UNDP, World Bank, E.: Post-Disaster Needs Assessments, 2013.
- [9] R. Gunasekera, J. Daniell, A. Pomonis, R.A.D. Arias, O. Ishizawa, H. Stone, Methodology Note on the Global RAPid Post-disaster Damage Estimation (GRADE) Approach, 2018.
- [10] B. Desai, A. Maskrey, P. Peduzzi, A. De Bono, C. Herold, Making Development Sustainable: the Future of Disaster Risk Management, Global Assessment Report on Disaster Risk Reduction, 2015.
- [11] UNISDR, Report of the Open-Ended Intergovernmental Expert Working Group on Indicators and Terminology Relating to Disaster Risk Reduction, 2016.
- [12] G. Pita, J.P. Pinelli, K. Gurley, J. Mitrani-Reiser, State of the art of hurricane vulnerability estimation methods: a review, *Nat. Hazards Rev.* 16 (2) (2015) 1–16, [https://doi.org/10.1061/\(ASCE\)NH.1527-6996.0000153](https://doi.org/10.1061/(ASCE)NH.1527-6996.0000153).
- [13] H. de Moel, M. van Vliet, J.C.J.H. Aerts, Evaluating the effect of flood damage-reducing measures: a case study of the unembanked area of Rotterdam, *The Netherlands, Reg. Environ. Change* (2013) 1–14, <https://doi.org/10.1007/s10113-013-0420-z>.
- [14] J. Li, B.F. Spencer, A.S. Elashai, Bayesian updating of fragility functions using hybrid simulation, *J. Struct. Eng.* 139 (7) (2013) 1160–1171, [https://doi.org/10.1061/\(ASCE\)ST.1943-541X.0000685](https://doi.org/10.1061/(ASCE)ST.1943-541X.0000685).
- [15] A.U. Abdelhady, S.M.J. Spence, J. McCormick, Risk and fragility assessment of residential wooden buildings subject to hurricane winds, *Struct. Saf.* 94 (2022) 102137, <https://doi.org/10.1016/j.strusafe.2021.102137>.
- [16] S. Chung Yau, N. Lin, E. Vanmarcke, Hurricane damage and loss estimation using an integrated vulnerability model, *Nat. Hazards Rev.* 12 (4) (2011) 184–189, [https://doi.org/10.1061/\(ASCE\)NH.1527-6996.0000035](https://doi.org/10.1061/(ASCE)NH.1527-6996.0000035).
- [17] J. Douglas, Physical vulnerability modelling in natural hazard risk assessment, *Nat. Hazards Earth Syst. Sci. Phys.* 7 (7) (2007) 283–288.
- [18] G.L. Pita, J.P. Pinelli, K.R. Gurley, S. Hamid, Hurricane vulnerability modeling: development and future trends, *J. Wind Eng. Ind. Aerod.* 114 (2013) 96–105, <https://doi.org/10.1016/j.jweia.2012.12.004>.
- [19] P. Wijayanti, X. Zhu, P. Hellegers, Y. Budiyo, E.C. van Ierland, Estimation of river flood damages in Jakarta, Indonesia, *Nat. Hazards* 86 (3) (2017) 1059–1079, <https://doi.org/10.1007/s11069-016-2730-1>.
- [20] F. Bono, E. Gutiérrez, A network-based analysis of the impact of structural damage on urban accessibility following a disaster: the case of the seismically damaged Port Au Prince and Carrefour urban road networks, *J. Transport Geogr.* (2011), <https://doi.org/10.1016/j.jtrangeo.2011.08.002>.
- [21] S. Koshimura, T. Oie, H. Yanagisawa, F. Imamura, Developing fragility functions for tsunami damage estimation using numerical model and post-tsunami data from Banda Aceh, Indonesia, *Coast Eng. J.* 51 (3) (2009) 243–273, <https://doi.org/10.1142/S0578563409002004>.
- [22] K. Kim, J. Davidson, Unmanned aircraft systems used for disaster management, *Transport. Res. Rec.* 2532 (2015) 83–90, <https://doi.org/10.3141/2532-10>.
- [23] J.A. de Bruijn, H. de Moel, B. Jongman, M.C. de Ruyter, J. Wagemaker, J.C.J.H. Aerts, A global database of historic and real-time flood events based on social media, *Sci. Data* 6 (1) (2019) 1–12.
- [24] M. Yu, C. Yang, Y. Li, Big data in natural disaster management: a review, *Geosciences* 8 (5) (2018), <https://doi.org/10.3390/geosciences8050165>.
- [25] H. Cho, M. Rivera-Sánchez, S.S. Lim, A multinational study on online privacy: global concerns and local responses, *New Media Soc.* 11 (3) (2009) 395–416, <https://doi.org/10.1177/1461444808101618>.
- [26] P.S. Koutsourelakis, Assessing structural vulnerability against earthquakes using multi-dimensional fragility surfaces: a Bayesian framework, *Probabilist. Eng. Mech.* 25 (1) (2010) 49–60, <https://doi.org/10.1016/j.probengmech.2009.05.005>.
- [27] S. Mishra, O.A. Vanli, B.P. Alduse, S. Jung, Hurricane loss estimation in wood-frame buildings using Bayesian model updating: assessing uncertainty in fragility and reliability analyses, *Eng. Struct.* (2017), <https://doi.org/10.1016/j.engstruct.2016.12.063>.
- [28] T. Rossetto, I. Ioannou, D.N. Grant, Existing empirical fragility and vulnerability relationships: compendium and guide for selection, *GEM Tech. Rep.* 1 (October) (2015) 77, <https://doi.org/10.13117/GEM.VULN-MOD.TR2015.01>.
- [29] R. Ospina, S.L.P. Ferrari, Inflated beta distributions, *Stat. Pap.* 51 (1) (2010) 111–126, <https://doi.org/10.1007/s00362-008-0125-4>.
- [30] W.R. Gilks, S. Richardson, D.J. Spiegelhalter, *Markov Chain Monte Carlo in Practice* Chapman & Hall: London, Markov Chain Monte Carlo Pract, Chapman Hall, London., 1996.

- [31] M. Plummer, JAGS: a program for analysis of Bayesian graphical models using Gibbs sampling, in: *Proceedings of the 3rd International Workshop on Distributed Statistical Computing*, vol. 124, 2003, pp. 1–10.
- [32] B.R. Ellingwood, D.V. Rosowsky, Y. Li, J.H. Kim, Fragility assessment of light-frame wood construction subjected to wind and earthquake hazards, *J. Struct. Eng.* 130 (12) (2004) 1921–1930.
- [33] K.H. Lee, D.V. Rosowsky, Fragility assessment for roof sheathing failure in high wind regions, *Eng. Struct.* 27 (6) (2005) 857–868.
- [34] Y. Li, B.R. Ellingwood, Hurricane damage to residential construction in the US: importance of uncertainty modeling in risk assessment, *Eng. Struct.* 28 (7) (2006) 1009–1018, <https://doi.org/10.1016/j.engstruct.2005.11.005>.
- [35] J. Holmes, Vulnerability curves for buildings in tropical-cyclone regions, in: *Probabilistic Mechanics & Structural Reliability*, 1996, pp. 78–81.
- [36] A.K. Gupta, S. Nadarajah, *Handbook of Beta Distribution and its Applications*, CRC press., 2004.
- [37] S.L.P. Ferrari, F. Cribari-Neto, Beta regression for modelling rates and proportions, *J. Appl. Stat.* 31 (7) (2004) 799–815, <https://doi.org/10.1080/0266476042000214501>.
- [38] S.A. Keote, D. Kumar, R. Singh, Construction of low rise buildings in cyclone prone areas and modification of cyclone, *J. Energy Power Sources* 2 (2015) 247–255.
- [39] J.M. Shultz, J. Russell, Z. Espinel, Epidemiology of tropical cyclones: the dynamics of disaster, disease, and development, *Epidemiol. Rev.* 27 (1) (2005) 21–35, <https://doi.org/10.1093/epirev/mxi011>.
- [40] M. Plummer, DSC 2003 Working Papers JAGS: A Program for Analysis of Bayesian Graphical Models Using Gibbs Sampling, 2003 [online] Available from: <http://www.ci.tuwien.ac.at/Conferences/DSC-2003/>.
- [41] M.K. Cowles, B.P. Carlin, Markov chain Monte Carlo convergence diagnostics: a comparative review, *J. Am. Stat. Assoc.* 91 (434) (1996) 883–904, <https://doi.org/10.1080/01621459.1996.10476956>.
- [42] S.P. Brooks, G.O. Roberts, Convergence assessment techniques for Markov chain Monte Carlo, *Stat. Comput.* 8 (4) (1998) 319–335, <https://doi.org/10.1023/A:1008820505350>.
- [43] L.A. Avila, S.R. Stewart, R. Berg, A.B. Hagen, National Hurricane Center Tropical Cyclone Report, 2020. Hurricane Dorian, Miami.
- [44] K.R. Knapp, M.C. Kruk, D.H. Levinson, H.J. Diamond, C.J. Neumann, The international best track archive for climate stewardship (IBTrACS), *Bull. Am. Meteorol. Soc.* 91 (3) (2010) 363–376, <https://doi.org/10.1175/2009BAMS2755.1>.
- [45] G.J. Holland, An analytic model of the wind and pressure profiles in hurricanes, *Mon. Weather Rev.* 108 (8) (1980) 1212–1218, [https://doi.org/10.1175/1520-0493\(1980\)108<1212:AAMOTW>2.0.CO;2](https://doi.org/10.1175/1520-0493(1980)108<1212:AAMOTW>2.0.CO;2).
- [46] N. Lin, D. Chavas, On hurricane parametric wind and applications in storm surge modeling, *J. Geophys. Res. Atmos.* 117 (D9) (2012), <https://doi.org/10.1029/2011JD017126>.
- [47] M. Powell, G. Soukup, S. Cocke, S. Gulati, N. Morisseau-Leroy, S. Hamid, N. Dorst, L. Axe, State of Florida hurricane loss projection model: atmospheric science component, *J. Wind Eng. Ind. Aerod.* 93 (8) (2005) 651–674, <https://doi.org/10.1016/j.jweia.2005.05.008>.
- [48] Department of Statistics, 2000 Census of Population and Housing, 2002. Nassau, Bahamas.
- [49] Department of Statistics, 2010 Census of Population and Housing, 2012. Nassau, Bahamas.
- [50] Department of Statistics, Population Projections 2010–2040, 2015. Nassau, Bahamas.
- [51] Department of Statistics, Report of the 2013 Household Expenditure Survey, 2016. Nassau, Bahamas.
- [52] Shanty Town Task Force, Abaco Shanty Town Assessment Report, 2018. Nassau, Bahamas.
- [53] Department of Statistics, Building Construction Statistics Report, 2018. Nassau, Bahamas.
- [54] A. Curtis, W.F. Fagan, Capturing damage assessment with a spatial video: an example of a building and street-scale analysis of tornado-related mortality in Joplin, Missouri, *Ann. Assoc. Am. Geogr.* 103 (6) (2013) 1522–1538.
- [55] M.A. Meyer, M.D. Hendricks, Using photography to assess housing damage and rebuilding progress for disaster recovery planning, *J. Am. Plann. Assoc.* 84 (2) (2018) 127–144.
- [56] C.C. Massarra, C.J. Friedland, B.D. Marx, J.C. Dietrich, Predictive multi-hazard hurricane data-based fragility model for residential homes, *Coast. Eng.* 151 (2019) 10–21, <https://doi.org/10.1016/j.coastaleng.2019.04.008>.
- [57] P.E. Shrout, J.L. Fleiss, Intraclass correlations: uses in assessing rater reliability, *Psychol. Bull.* 86 (2) (1979) 420.
- [58] J.L. Fleiss, Measuring nominal scale agreement among many raters, *Psychol. Bull.* 76 (5) (1971) 378.
- [59] UNISDR, Global Assessment Report on Disaster Risk Reduction 2015, 2015 [online] Available from: <https://www.unisdr.org/we/inform/publications/42809>.
- [60] P.J. Vickery, P.F. Skerj, J. Lin, L.A. Twisdale, M.A. Young, F.M. Lavelle, HAZUS-MH hurricane model methodology. II: damage and loss estimation, *Nat. Hazards Rev.* 7 (2) (2006) 94–103, [https://doi.org/10.1061/\(ASCE\)1527-6988\(2006\)7:2\(94\)](https://doi.org/10.1061/(ASCE)1527-6988(2006)7:2(94)).
- [61] Eclac, Idb, Paho, Who, Assessment of the Effects and Impacts of Hurricane Dorian in the Bahamas, 2019.
- [62] M. Duggan, J. Brenner, The Demographics of Social Media Users, 2012, Pew Research Center's Internet & American Life Project, Washington, DC, 2013.
- [63] B. Miles, S. Morse, The role of news media in natural disaster risk and recovery, *Ecol. Econ.* 63 (2–3) (2007) 365–373, <https://doi.org/10.1016/j.ecolecon.2006.08.007>.
- [64] T. Weyand, I. Kostrikov, J. Philbin, Planet-photo geolocation with convolutional neural networks, in: *European Conference on Computer Vision*, 2016, pp. 37–55.
- [65] S. Naito, H. Tomozawa, Y. Mori, T. Nagata, N. Monma, H. Nakamura, H. Fujiwara, G. Shoji, Building-damage detection method based on machine learning utilizing aerial photographs of the Kumamoto earthquake, *Earthq. Spectra* 36 (3) (2020) 1166–1187, <https://doi.org/10.1177/8755293019901309>.
- [66] A. Hatzikyriakou, N. Lin, J. Gong, S. Xian, X. Hu, A. Kennedy, Component-based vulnerability analysis for residential structures subjected to storm surge impact from Hurricane Sandy, *Nat. Hazards Rev.* 17 (1) (2016) 5015005.
- [67] D.V. Cicchetti, Guidelines, criteria, and rules of thumb for evaluating normed and standardized assessment instruments in psychology, *Psychol. Assess.* 6 (4) (1994) 284.
- [68] T.K. Koo, M.Y. Li, A guideline of selecting and reporting intraclass correlation coefficients for reliability research, *J. Chiropr. Med.* 15 (2) (2016) 155–163, <https://doi.org/10.1016/j.jcm.2016.02.012>.
- [69] J.R. Landis, G.G. Koch, The measurement of observer agreement for categorical data, *Biometrics* 159–174 (1977).
- [70] Matthew Mason S., Korah Parackal I., Vulnerability of buildings and civil infrastructure to tropical cyclones: a preliminary review of modelling approaches and literature, *Bushfire and Natural Hazards CRC* (2015).
- [71] Daniel Smith J., Mark Edwards, Korah Parackal, John Ginger, David Henderson, Hyeuk Ryu, Martin Wehner, Modelling vulnerability of Australian housing to severe wind events: past and present, *Austr. J. Struct. Eng.* (2020), <https://doi.org/10.1080/13287982.2020.1744900>. In press.
- [72] George Walker R., Modelling the vulnerability of buildings to wind—a review, *Canadian Journal of Civil Engineering* (2011).